Analytical results for cell constriction dominated by bending energy

Victor G. Almendro-Vedia,[1] Francisco Monroy,[2] and Francisco J. Cao[1,*]

[1]*Departamento de Física Atómica, Molecular y Nuclear, Universidad Complutense de Madrid, 28040 Madrid, Spain*

[2]*Departamento de Química Física I, Universidad Complutense de Madrid, 28040 Madrid, Spain*

(Received 15 July 2014; revised manuscript received 13 October 2014; published 28 January 2015)

Analytical expressions are obtained for the main magnitudes of a symmetrically constricted vesicle. These equations provide an easy and compact way to predict minimal requirements for successful constriction and its main magnitudes. Thus, they can be useful for the design of synthetic divisomes and give good predictions for magnitudes including constriction energy, length of the constriction zone, volume and area of the vesicle, and the stability coefficient for symmetric constriction. The analytical expressions are derived combining a perturbative expansion in the Lagrangian for small deformations with a cosine ansatz in the constriction region. Already the simple fourth-order (or sixth-order) approximation provides a good approximation to the values of the main physical magnitudes during constriction, as we show through comparison with numerical results. Results are for vesicles with negligible effects from spontaneous curvature, surface tension, and pressure differences. This is the case when membrane components generating spontaneous curvature are scarce, membrane trafficking is present with low energetic cost, and the external medium is isotonic

DOI: 10.1103/PhysRevE.91.012713 PACS number(s): 87.17.Ee, 87.17.Rt, 87.15.ad

I. INTRODUCTION

Cell division involves membrane constriction forces forming a saddle-shaped neck that separates the two lobes that eventually pinch off to produce the two daughter cells [1–4]. The mechanics of cell constriction is a crucial problem of bioenergetics that directly deals with the membrane forces required to distort the cell along a stable cytokinetic pathway [5–8]. In the simplest model, the whole cell is depicted as a membrane vesicle where bending forces produce constriction of an initial sphere into a deformed two-lobed configuration. When only bending forces, but not membrane tension or turgor forces, are considered, the model describes a growing cell membrane that is able to exchange lipid material with its metabolic reservoir and is osmotically controlled into the tensionless state, a set of conditions compatible with the dividing cell. In a previous paper [9] the energetics of constriction were calculated by following a variational approach to the minimization problem of the bending energy in the case of the tensionless and turgor-free vesicle. As variational proof functions we take linear combinations of trigonometric functions, the vesicle shapes were optimized by minimizing the bending energy along a continuous constriction pathway defined as the monotonic decrease of the neck radius. From that approach, the constriction forces and the optimal geometrical parameters were calculated from the minimal variational energies along the constriction pathway. Amazingly, the zeroth-order variational solution selected was revealed to be extremely efficient in approaching the exact solution in a broad range of membrane constrictions from the initial spherical state. Based on that result, we decided to take advantage of such solutions as an ansatz and compute the constriction perturbative orders in a framework from which analytic expressions to the more relevant properties such as constriction zone length L_m, bending energy, surface area, and volume can be derived. These analytic expressions are given in terms of the scaling parameters that define the geometry of the constriction neck, namely, the maximum radius R_m and the constriction ratio $s = (R_m - R_c)/R_m$ (see Fig. 1). In this paper we obtain a set of analytic formulas that, already at leading order, accurately describe the bending energetics in the limit of small constrictions. The dominant terms are obtained as power laws of the radial constriction s with amplitudes depending on the other system parameters. The perturbative expansion provides us with progressively accurate approaches to the exact values of the relevant properties. The exact values are calculated as the numerical solutions of the corresponding Euler-Lagrange equations to determine the accuracy of the analytical results. We present three paradigmatic cases: the constant maximum radius, the constant volume, and the constant area. Constriction at a constant maximum radius resembles the conditions encountered in rod-shaped cells with a cell wall as in *E. Coli* (if additional invariable cylindrical membranes are added to each side of the constriction region) [3,10]. Constriction at a constant volume resembles the conditions encountered in cells without a cell wall and with intense membrane trafficking (which allows them to produce the additional area required under these conditions) [11–14]. Constriction at a constant area resembles the conditions that will take place for a cell that has some disturbance that inhibits membrane trafficking [15–17]. (In addition, rescaling of the results will also allow one to obtain the values of magnitudes along any pathway of volume or area changes during constriction.) The results are discussed from a biological perspective in the context of the physical mechanisms underlying the common mechanical pathways of cell division.

II. METHODS

A. Elastic energy of a tensionless vesicle: Bending Hamiltonian

Changing the shape of a spherical vesicle from its equilibrium configuration is a nonspontaneous process that requires an input of energy. In the minimal description, in the

*Corresponding author: francao@fis.ucm.es

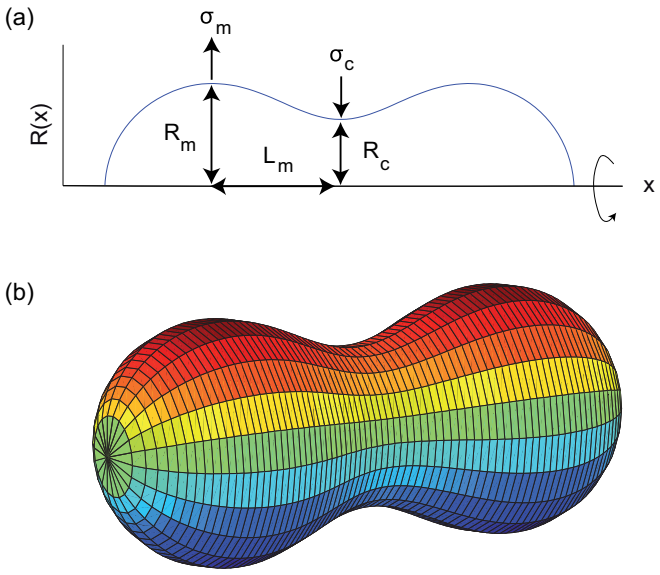

FIG. 1. (Color online) (a) Profile $R(x)$ of an axisymmetric and symmetrically constricted vesicle and its characteristic parameters. (b) Surface resulting from the revolution around the x axis of the previous profile $R(x)$.

absence of tensional fields on the membrane, the energy of the vesicle deformations is assumed to exclusively involve bending elasticity of a two-dimensional sheet, particularly contributions from mean and Gaussian curvatures [5]

$$E_b = E_m + E_G = \frac{1}{2}\kappa \int (C_1 + C_2 - C_0)^2 dA + \kappa_G \int C_1 C_2 dA. \quad (1)$$

In this equation κ is the bending modulus, κ_G is the Gaussian bending rigidity, Ω is the surface that defines the membrane, dA is its element of area, C_1 and C_2 are its local principal curvatures, and the parameter C_0 is the spontaneous curvature (which effectively accounts for possible asymmetries in the membrane structure between the inner and the outer sides). In the case $C_0 = 0$, the membrane in the flat configuration defines the absolute minimum of bending energy. In the particular case of the sphere ($C_1 = C_2 = 1/R_0$), the bending energies are $E_m^{(\mathrm{sph})} = 8\pi\kappa$ and $E_G^{(\mathrm{sph})} = 4\pi\kappa_G$ for the mean and Gaussian contributions, respectively. In general, any change of the membrane shape makes the total bending energy in Eq. (1) vary. However, the integrated Gaussian curvature [the second term in Eq. (1)] is invariant under shape changes that do not change topology, as stated by the Gauss-Bonet theorem [5]. Since the constriction process in a sphere does not change its topology and only involves shapes that are topologically equivalent to the initial sphere (for $s < 1$), the integrated Gaussian energy remains constant at $E_G = E_G^{(\mathrm{sph})} = 4\pi\kappa_G$, independently of the size and shape of the system. Consequently, to analyze the mechanics of constriction we must just deal with the variations of energy due to changes in mean curvature E_m, which is independent on the size of the system for zero spontaneous curvature $C_0 = 0$. In the special case of surfaces of revolution with a rotation symmetry axis along x, if the surface is represented in Cartesian coordinates as $\boldsymbol{r} = [x, y, h(x,y)]$, where $h(x,y)$ represents the surface profile as an height over the $x - y$ plane, one gets

$$h(x,y) = \pm\sqrt{R^2(x) - y^2}, \quad (2)$$

with $R(x)$ being the functional form describing the membrane profile in the x-z plane. For this parametrization, the mean curvature of this surface becomes

$$\frac{C_1 + C_2}{2} = \frac{R_{xx}R - 1 - R_x^2}{2R\left(1 + R_x^2\right)^{3/2}}. \quad (3)$$

Note that this result is independent of the coordinate y, as corresponds to rotational symmetry around x. The element of area is

$$dA = R\sqrt{\frac{1 + R_x^2}{R^2 - y^2}}\,dx\,dy. \quad (4)$$

Consequently, once the membrane profile $R(x)$ is known between the two extremes x_i and x_f, the bending energy for the surface of revolution is given by

$$E_m(x_i, x_f) = \pi\kappa \int_{x_i}^{x_f} K_m(x)dx, \quad (5)$$

with

$$K_m(x) = \frac{\left(1 + R_x^2 - R_{xx}R\right)^2}{R\left(1 + R_x^2\right)^{5/2}}. \quad (6)$$

The vesicle takes the shape that minimizes this bending energy E_m (up to thermal effects). In this paper, we restrict the study to the case of zero spontaneous curvature $C_0 = 0$, negligible tension $\Sigma = 0$, and no pressure difference between internal and external environments $\Delta p = 0$. Thus, the bending energy becomes size invariant, a property that simplifies the calculations drastically, as it implies no dependence of the bending energy on the system size. This means that once we have determined the shape that minimizes the energy, its transformation under an overall dilatation leads to a shape that has the same energy and also minimizes the energy. This property will be very useful in this paper. Indeed, it allows one to recall that under an overall dilatation, i.e., $x \to \lambda x$ and $R \to \lambda R$, the area is transformed as $A \to \lambda^2 A$ and the volume as $V \to \lambda^3 V$.

B. Perturbative method

In the present problem, an initially spherical vesicle is deformed under a radial force exerted as a constriction ring at its equator. Then a saddle-shaped neck is formed, separating two quasispherical lobes (see Fig. 1). As constriction proceeds, the neck progressively narrows and the vesicle lobes evolve up to final binary fission into two separate daughter spheres. We will take advantage of the perturbative method to get approximate formulas of the elastic energy corresponding to the constricted configurations calculated with respect to the unconstricted (i.e., unperturbed) configuration [18]. Our unconstricted initial configuration is a sphere of radius R_m, so constriction is assumed to proceed by keeping this maximum radius R_m constant (see Fig. 1). This can be realized if the deformation effect of the contents of the vesicle (or cell) is represented as an effective line tension towards the exterior σ_m,

which keeps the maximum radius R_m constant. This requires the two polar caps to be hemispheres of radius R_m during the whole constriction process, thus they do not change their bending energy. Therefore, all bending energy changes arise from the central constriction region that changes from R_m to a profile $R_c(x,s)$, where the variable

$$s = (R_m - R_c)/R_m \tag{7}$$

defines the constriction ratio ($s \in [0, 1]$), i.e., the ratio between the maximum radius R_m and the constriction radius R_c (see Fig. 1). The constriction profile $R(x) \approx R_0(x,s)$ provides us with the respective derivatives R_x and R_{xx} needed to compute the integrand K_m [Eq. (6)] of the energy. In order to apply the perturbative method, it is convenient to define the small deformation function

$$u(x,s) = R_m - R_0(x,s). \tag{8}$$

The function $K_m\{u[f(x)]\}$ can now be expanded in terms of the small deformation $u\,(x,s)$ and of its first- and second-order derivatives (u_x,u_{xx}), which depend on the x coordinate and the constriction ratio s and can, in general, be calculated as a function of the scaling parameters R_m and L_m. In order to calculate the elastic energy, the function K_m is expanded up to the nth order of perturbation

$$K_m[f_0(u)] \approx K_0 + K_1 u_i + K_2 u_i^2 + \cdots + K_n u_i^n + o\left(u_i^{n+1}\right).$$

When this simplified integrand is included as the kernel of the elastic energy in Eq. (6) and the integration is performed between the two extremal limits defining the complete surface ($x_i = 0$ and $x_f = L_m$; see Fig. 1), the resulting expression can be minimized, giving a Euler-Lagrange equation for u, analogously to the computation in Ref. [18].

If an appropriate ansatz is additionally assumed for $R_0(x,s)$ in the interval $[0,L_m]$, the integrand becomes simpler and approximate analytical expression for the energy can be obtained. The energy $E_m = E_m(s,L_m,R_m,\kappa)$ depends on the mechanical parameter κ (the bending energy), on the size-scaling parameter R_m (the maximum radius), and on the variational parameters introduced by the ansatz, in our case only L_m (the length of the constriction region). Finally, energy minimization with respect to L_m provides its optimal value for a given constriction ratio s (recall that R_m stays constant along constriction),

$$\left[\frac{\partial E_m(s,L_m,R_m,\kappa)}{\partial L_m}\right]_s = 0 \Rightarrow L_m = L_m^{(\mathrm{opt})}(s). \tag{9}$$

This condition determines the approximate expression for the energy $E_m = E_m(s,L_m^{(\mathrm{opt})}(s),R_m,\kappa)$ as a function of the constriction ratio and the system parameters R_m and κ. With this result for $L_m^{(\mathrm{opt})}(s)$, approximate expressions for other magnitudes such as the area and volume can be obtained by performing a similar perturbative expansion for the integrands. These expressions have the form of a perturbative expansion for small constriction ratio s, as small deformations u imply small constriction ratio s.

C. Exact numerical solution: Euler-Lagrange equations

Another way to get the shapes of minimal energy of a vesicle during the constriction process is to numerically solve the corresponding Euler-Lagrange equations. General methods have been developed to calculate the equilibrium shapes of vesicles under different conditions. Here we follow the methodology in Refs. [19,20] and apply it to axisymmetric shapes stressed upon equatorial constriction, while the maximum radius remains constant. (See Appendix A for a brief summary of the numerical procedure.)

Maintaining the boundary conditions of radii R_m and R_c requires line tensions σ_m and σ_c, respectively. They act in opposite directions: Increasing σ_c forces R_c to decrease, thus increasing constriction, which requires an increase of σ_m to maintain constant R_m during the constriction process. Once the line tensions are known, the energetics of the system can also be addressed. For example, the energy due to line tension at the site of constriction will be

$$E_{\sigma_c} = 2\pi R_c \sigma_c, \tag{10}$$

a relationship that will be used below to calculate the forces exerted along the constriction process.

III. RESULTS

A. Tensionless vesicle with no spontaneous curvature

We obtain the perturbative expansion for the tensionless vesicle ($\Sigma = 0$) without pressure differences ($\Delta p = 0$) and for zero spontaneous curvature ($C_0 = 0$). In this case the only contribution to the energy is given by the mean curvature with $C_0 = 0$ [Eqs. (5) and (6)]. Since $u_x = -R_x$, $u_{xx} = -R_{xx}$ by the definition made in Eq. (8), the Taylor expansion up to tenth order of the integrand kernel of the mean curvature energy [Eq. (6)] reads

$$\begin{aligned}
K_m(u,u_x,u_{xx};R_m) \approx\ & \frac{1}{R_m}u^0 + \frac{1}{R_m^2}u + 2u_{xx} + \frac{1}{R_m^3}u^2 - \frac{1}{2R_m}u_x^2 + R_m u_{xx}^2 + \frac{1}{R_m^4}u^3 - \frac{1}{2R_m^2}uu_x^2 - uu_{xx}^2 - 3u_x^2u_{xx} + \frac{1}{R_m^5}u^4 \\
& - \frac{1}{2R_m^3}u^2u_x^2 + \frac{3}{8R_m}u_x^4 - \frac{5R_m}{2}u_x^2u_{xx}^2 + \frac{1}{R_m^6}u^5 - \frac{1}{2R_m^4}u^3u_x^2 + \frac{3}{8R_m^2}uu_x^4 + \frac{5}{2}uu_x^2u_{xx}^2 + \frac{15}{4}u_x^4u_{xx} \\
& + \frac{1}{R_m^7}u^6 - \frac{1}{2R_m^5}u^4u_x^2 + \frac{3}{8R_m^3}u^2u_x^4 - \frac{5}{16R_m}u_x^6 + \frac{35R_m}{8}u_x^4u_{xx}^2 + \frac{1}{R_m^8}u^7 - \frac{1}{2R_m^6}u^5u_x^2 + \frac{3}{8R_m^4}u^3u_x^4 \\
& - \frac{5}{16R_m^2}uu_x^6 - \frac{35}{8}u_x^6u_{xx} - \frac{35}{8}uu_x^4u_{xx}^2 + \frac{1}{R_m^9}u^8 - \frac{1}{2R_m^7}u^6u_x^2 + \frac{3}{8R_m^5}u^4u_x^4 - \frac{5}{16R_m^3}u^2u_x^6 + \frac{35}{128R_m}u_x^8
\end{aligned}$$

$$-\frac{105R_m}{16}u_x^6u_{xx}^2+\frac{1}{R_m^{10}}u^9-\frac{1}{2R_m^8}u^7u_x^2+\frac{3}{8R_m^6}u^5u_x^4-\frac{5}{16R_m^4}u^3u_x^6+\frac{35}{128R_m^2}uu_x^8+\frac{105}{16}uu_x^6u_{xx}^2$$
$$+\frac{315}{64}u_x^8u_{xx}+\frac{1}{R_m^{11}}u^{10}-\frac{R_m}{2R_m^9}u^8u_x^2+\frac{3}{8R_m^7}u^6u_x^4-\frac{5}{16R_m^5}u^4u_x^6+\frac{35}{128R_m^3}u^2u_x^8-\frac{63}{256R_m}u_x^{10}$$
$$+\frac{1155R_m}{128}u_x^8u_{xx}^2+o\left(u_i^{11}\right). \tag{11}$$

In a previous paper [9], using a variational approach to describe constriction mechanics, families of shape functions were proposed to describe the constriction region for $\Sigma=0$, $p=0$, and $C_0=0$. The assumed zeroth- order function family was [9]

$$R_0(x,s)=R_m\left\{1-\frac{s}{2}\left[1+\cos\left(\frac{\pi x}{L_m}\right)\right]\right\}, \tag{12}$$

where R_m is the maximal radius and L_m is the longitudinal distance between the center of the constriction neck (where the origin is placed) and the position where the radius is maximal. This simple zeroth-order family has proven to give good approximations for low constriction in a variational framework [9].

Here we combine this simple shape expression with the perturbative results to obtain approximate analytical expressions. Thus, we substitute

$$u(x,s)=R_m-R_c(x,s)=(R_m/2)s[1+\cos(\pi x/L_m)]$$

in Eq. (11). Then, integrating the resulting kernel between $x_i=0$ and $x_f=L_m$,

$$E_m(s,L_m)\approx 2\pi\kappa\int_0^{L_m}K_m[u(x,s),R_m]dx, \tag{13}$$

we obtain an approximate analytical expression for the bending energy, which does not depend on the vesicle size (R_m cancels out after integration, in the case of $C_0=0$, $p=0$, and $\Sigma=0$).

1. Neck dimensions

After integration, the bending energy is minimized with respect to L_m [see Eq. (9)]. This allows one to obtain the analytical expression for the optimal dimensions that define the shape of minimal bending energy for each constriction stage, characterized by s. The perturbative expansion for the optimal value of $L_m(s)$ takes the explicit form

$$\frac{L_m(s)}{R_m}\approx\frac{\pi 6^{1/4}}{2}\sqrt{s}\left[1-\frac{144+31\sqrt{6}}{576}s-\frac{4327+1488\sqrt{6}}{110\,592}s^2-\cdots\right], \tag{14}$$

which, for simplicity, is written here as the leading term scaling as $L_m(s)/R_m\sim s^{1/2}$ multiplied by the corresponding terms only up to fourth order in the perturbative expansion of the energy integrand (see Appendix B for higher-order expressions).

The leading term describes the small constriction region ($s\to 0$) and is found to scale as $L_m(s)/R_m\approx\alpha_0 s^{1/2}$, with a size-invariant coefficient characterized by a dimensionless amplitude $\alpha_0=6^{1/4}\pi/2\approx 2.46$. Higher terms are straightforwardly obtained by extending the Taylor expansion for small u in the energy integrand. The expansion coefficients are found to decrease strongly with the order of their term, which makes the series expansion rapidly convergent. This rapid convergence of the series and the comparison of the different orders with exact results [see Fig. 2(a)] confirm the robustness and stability of the present perturbative approach. Figure 2(a) shows a graphical plot of the s dependence of the perturbative formula in Eq. (14). The asymptotic leading term accurately describes the regime of small constrictions ($L_m/R_m\approx 2.46s^{1/2}$ at $s\leqslant 0.1$), while

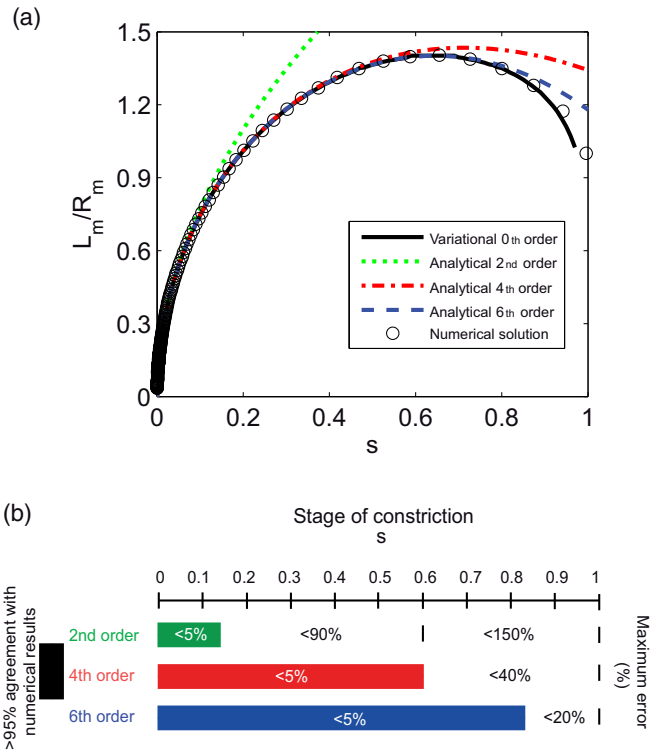

FIG. 2. (Color online) (a) Aspect ratio of the constriction region L_m/R_m as a function of the stage of constriction given by the constriction ratio s. Comparison of the exact results from numerical computations with the approximate results from the zeroth-order variational approximation and for analytical expressions obtained from several orders of perturbation for small deformations. (b) Validity of the results for L_m/R_m assuming a numerical solution as the exact solution. Each color represents a different order of the perturbative expansion for the analytical expression for L_m, as represented in Fig. 3(a). Thick lines show the limit values of s where these approximations can be used within an error lower than 5% (compared with numerical results). Outside these ranges of s, the maximum error is indicated in percentages.

higher perturbative terms contribute with negative components that approach the exact solution through a monotonic convergence. The exact result given by the numerical solution of the Euler-Lagrange equations (see the method described in Sec. II C for the case of $\Delta p = 0$, $\Sigma = 0$, and $C_0 = 0$) is represented for comparison.

In Fig. 2 the analytical expressions for different orders are observed to rapidly and monotonically converge to the zeroth-order variational result, which, for this magnitude, gives a good result when compared to the exact result found numerically. The quantitative fitness of the approximation is shown in Fig. 2(b), which plots the range of validity of each order of the analytic expression and compares their overall degree of agreement with respect to the exact solution. The fourth-order expression describes (with 95% agreement) the exact solution up to constrictions as large as $s \leqslant 0.8$, its maximal error being lower than 20% in describing the whole constriction path. Such a strong convergence is due to the high reliability of the ansatz used [see Eq. (12)], which is extremely efficient in describing the exact result, as evidenced when barely introduced in a variational schema [see Fig. 2(a), black line] [9]. For low constriction, $L_m/R_m \approx 2.5 s^{1/2} \gg s = (R_m - R_c)/R_m$, i.e., the length of the constriction region grows faster than the constriction depth. Thus the present result indicates an initial large longitudinal dilation due to localized equatorial constriction.

2. *Bending energy and constriction force*

Once the parameter L_m that minimizes the energy has been calculated [Eq. (14)], its value can be substituted in the equation for the bending energy [Eq. (13)], obtaining the approximate analytical formula for the increase in bending energy due to constriction

$$\frac{\Delta E_b}{8\pi\kappa} \approx \frac{\pi 6^{1/4}}{6}\sqrt{s}\left[1 + \frac{48 - 11\sqrt{6}}{192}s + \frac{7439 - 1584\sqrt{6}}{36\,864}s^2 - \cdots\right], \qquad (15)$$

where $\Delta E_b = E_m(s) - E_m(s=0)$ with $E_m(s=0) = E_m^{(\mathrm{sph})} = 8\pi\kappa$. This expression is up to fourth order in the perturbative expansion; higher-order formulas are collected in Appendix B. The results for the bending energy are graphically compared in Fig. 3.

The leading term at low constriction ($s < 0.1$) in the analytical expression $\Delta E_b^{(0)}/8\pi\kappa \approx (6^{1/4}\pi/6)s^{1/2}$ has the same $s^{1/2}$ scaling as the exact result (numerical solution), as shown by the double-logarithmic plot (see the inset in Fig. 3). This indicates that the leading term in the analytic solution closely describes the exact solution, at least at low degrees of constriction. This leading term indeed gives good predictions at the low-constriction regime ($s < 0.3$) with errors smaller than 10%. Even for higher constrictions, the leading-order expression gives good order of magnitude estimates, with a maximum final value similar to the bending energy of the initial sphere, which is $\Delta E_b / E_m^{(\mathrm{sph})} = 6^{1/4}\pi/6 = \alpha_0/3 \approx 0.82$ for $s \to 1$. Incidentally, the fourth-order perturbation written in Eq. (15) nearly matches the exact value, predicting the doubling of the bending energy, i.e., $\Delta E_b / E_m^{(\mathrm{sph})} \approx 1$ for $s \to 1$. As expected,

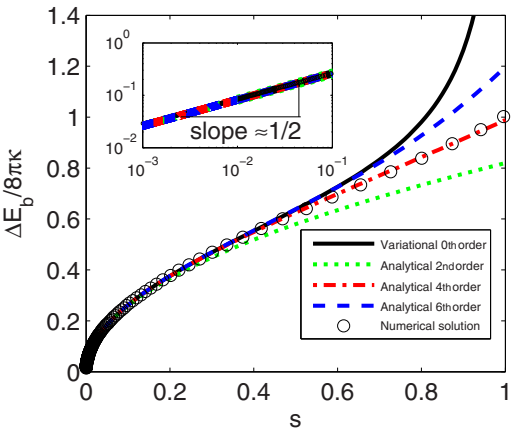

FIG. 3. (Color online) Bending energy increase as a function of the stage of constriction given by the constriction ratio s. (The value of the mean curvature contribution to bending energy in a sphere is in units of $8\pi\kappa$.) Comparison of the exact numerical results with the approximate zeroth-order variational results and several orders of the analytical expressions obtained through perturbative methods plus an ansatz. The top left inset shows numerical results on a logarithmic scale to stress the leading-order scaling with the constriction ratio s, which agrees with the prediction of the leading-order (second-order) analytical expression.

higher-order expressions for the energy converge to the energy curve obtained with the zeroth-order variational solution in Eq. (12) (see Fig. 3). Basically, the formulas obtained are accurate to analytically describe the energy corresponding to the zeroth-order variational results in Ref. [9]. More accurate solutions for the bending energy in the high-constriction regime ($s > 0.65$) should require solutions more precise than Eq. (12), i.e., a better accounting for the strong changes of curvature occurring in the constriction region. However, incidentally the fourth-order analytical expression is better for this magnitude, the bending energy, than its corresponding zeroth-order variational solution.

It is worth mentioning the doubling of the bending energy existing at maximal constriction ($\Delta E_b / E_m^{(\mathrm{sph})} \to 1$ at $s \to 1$). It implies that the mean curvature contribution to the bending energy is that of two spheres. However, we recall that an additional Gaussian curvature energy contribution of $4\pi\kappa_G \approx 100 k_B T$, due to the change in topology involved, will be needed to split the maximal constricted vesicle into two spherical ones [21].

As far as the bending energy is known as a function of the constriction rate, the constriction force can be calculated as

$$F_c \equiv -\frac{dE_m}{dR_c} = -\frac{dE_m}{ds}\frac{ds}{dR_c} = \frac{1}{R_m}\frac{dE_m}{ds}. \qquad (16)$$

Thus, the analytic formula for the constriction force can be obtained in a straightforward way as the derivative of the bending energy with respect to the constriction ratio

$$F_c(s) \approx \frac{2\pi^2 6^{1/4}}{3}\frac{\kappa}{R_m}\frac{1}{\sqrt{s}}\left[1 + \left(\frac{48 - 11\sqrt{6}}{64}\right)s + 5\left(\frac{7439 - 1584\sqrt{6}}{36\,864}\right)s^2 - \cdots\right]. \qquad (17)$$

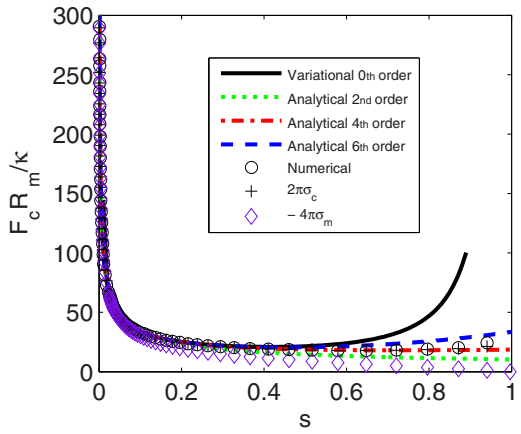

FIG. 4. (Color online) Constriction force F_c (in units of R_m/κ) at all stages of constriction. Comparison of the exact numerical results with the approximate zeroth-order variational results and the analytical expressions obtained with several orders of perturbative expansion. Plotted are $F_c \approx 2\pi\sigma_c$, where σ_c is the line tension at the constriction site (numerically computed), and $4\pi\sigma_m$, where σ_m is the line tension at the maximum radius site (numerically computed). (For the procedure for the numerical computation of the line tensions see Appendix A.)

This expression is written up to fourth order in the perturbative expansion of the energy integrand (for higher-order expressions see Appendix B). As expected from a dimensional argument, constriction forces with an amplitude of the order of κ/R_m are predicted by Eq. (17). The dominant term is found to scale as $F_c \sim (\kappa/R_m)s^{-1/2}$, i.e., the smaller the vesicle, the higher its bare curvature and thus the higher the force required for a given constriction.

The fourth-order formula describes accurately the results up to $s = 0.9$. Higher-order terms, however, introduce larger errors in the description of the constriction forces, as expected from convergence towards the zeroth-order variational solution at high constriction (analogous to the results for bending energy).

As described in Appendix A, Fig. 4 also shows $F_c \approx 2\pi\sigma_c = dE_{\sigma_c}/dR_c$ (in units of R_m/κ), where E_{σ_c} is given by Eq. (A1) and the line tension σ_c is computed from the jump in γ at the constriction site in the numerical computation (A4). This shows the consistency of the two ways of computing the constriction force. The line tension to keep the maximum radius σ_m is also shown and we found $-2\sigma_m \leqslant \sigma_c$.

3. *Vesicle area and volume during constriction*

The perturbation approach has provided us with an analytical formula for the dimensional ratio L_m/R_m from which the relevant vesicle dimensions can be calculated, particularly the membrane area and the volume enclosed. Let us start with the membrane area. For a given shape $R(x)$, the area sustained by its revolution surface around the x axis is given by

$$A = 2\pi \int_{x_i}^{x_f} R\sqrt{1 + R_x^2}\,dx. \tag{18}$$

In order to apply the perturbation method, we operate similarly as with the bending energy: $R(x)$ is replaced by the small-$u(x)$ variable [Eq. (8)] and the integrand in Eq. (18) is expanded in a Taylor series in $u(x)$ up to sixth order:

$$R\sqrt{1 + R_x^2} \approx R_m - u + \frac{R_m}{2}u_x^2 - \frac{1}{2}uu_x^2 - \frac{R_m}{8}u_x^4 + \frac{1}{8}uu_x^4 + \frac{R_m}{16}u_x^6 - \frac{1}{16}uu_x^6 - \frac{5R_m}{128}u_x^8 + o(u_i^9). \tag{19}$$

Then the cosine ansatz for the shape [Eq. (12)] is replaced and integration is performed between the limits $x_i = 0$ and $x_f = L_m$, with L_m given by Eq. (14). Assuming a constant maximum radius R_m, the increase of area during constriction is

$$\frac{\Delta A(s)}{A_0} \approx \frac{\pi 6^{1/4}}{2}\sqrt{s}\left[1 - \frac{432 + 7\sqrt{6}}{576}s + \frac{10\,121 + 336\sqrt{6}}{110\,592}s^2 + \cdots\right], \tag{20}$$

where $\Delta A(s) = A(s) - A(s = 0)$ with $A(s = 0) = A_0 = 4\pi R_m^2$. This expression is of fourth order in the perturbative expansion and a higher-order formula can be found in Appendix B.

The result in Eq. (20) establishes a direct relation between the longitudinal elongation of the vesicle and its membrane dilation. In the asymptotic regime, at small constriction, the dominant term in Eq. (20) equals that of the optimal L_m/R_m ratio given by Eq. (14), which is $\Delta A/A_0 = L_m/R_m$ at $s \to 0$. This means that a near-cylindrical neck with length $2L_m$ is formed at the initial stages of constriction; in that case, one expects a relative increase of area $(\Delta A/A)_{\rm cyl} = (2\pi R_m) \times (2L_m)/4\pi R_m^2 = L_m/R_m$, as quoted. Figure 5 shows the accuracy of the approximate analytical result for the membrane dilation required for constriction with constant R_m. In this case, although the leading-order (second-order) expression only gives good results for very small constrictions ($s \leqslant 0.075$), the fourth-order expression greatly improves convergence (see Fig. 5). As expected from previous features, higher-order

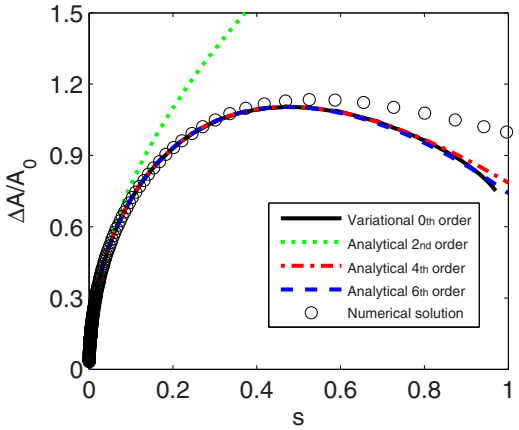

FIG. 5. (Color online) Relative change in area $\Delta A(s)/A_0$ versus constriction ratio s along the whole path of constriction keeping constant the maximum radius R_m. Comparison of the exact numerical results with the approximate zeroth-order variational results and the analytical expressions obtained with several orders of perturbative expansion.

perturbative expressions converge to the variational solution, but do not describe better the exact result at high constrictions ($s > 0.5$).

A similar calculation can be performed to evaluate the increase of volume occurring upon constriction at constant maximum radius R_m. For a surface of revolution, the enclosed volume is given by

$$V = \pi \int_{x_i}^{x_f} R^2 dx. \tag{21}$$

If the integrand is expressed in terms of the small variable $u[R(x)]$, then one obtains the exact formula $R^2 = (R_m - u)^2 = u^2 - 2R_m u + R_m^2$. Replacing it in Eq. (21) and doing the integration between the limits $x_i = 0$ and $x_f = L_m$, with L_m given by its expansion in Eq. (14), one gets the following analytic expression for the increase of volume

$$\frac{\Delta V(s)}{V_0} \approx \frac{3\pi 6^{1/4}}{4}\sqrt{s}\left[1 - \frac{31\sqrt{6}+720}{576}s + \frac{4464\sqrt{6}+64\,793}{110\,592}s^2 + \cdots\right], \tag{22}$$

where $\Delta V(s) = V(s) - V(s=0)$ with $V(s=0) = V_0 = 4\pi R_m^3/3$. (As for other magnitudes, this is a fourth-order perturbation expression; a higher-order formula can be found in Appendix B.)

Analogously to the other dimensional properties, a $\Delta V/V \sim s^{1/2}$ scaling is found for the increase of volume of the vesicle inflated under the action of the constriction deformation. From a comparison of the amplitudes of the dominant terms, the following mutual proportionality relationship can be stated among the different dimensional properties: $\Delta A/A = \frac{2}{3}(\Delta V/V) = L_m/R_m$ at $s \to 0$. Again, assuming the formation of a cylindrical neck of length $2L_m$ at small constriction, one expects a relative increase of volume $(\Delta V/V)_{\text{cyl}} = (\pi R_m^2) \times (2L_m)/(4\pi R_m^3/3) = \frac{3}{2}(L_m/R_m)$, as found.

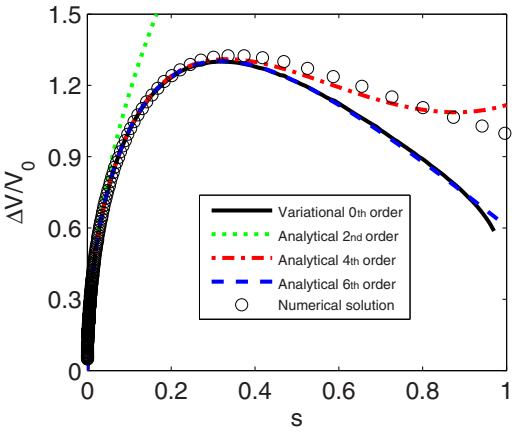

FIG. 6. (Color online) Relative change in volume $\Delta V(s)/V_0$ along the whole path of constriction keeping constant the maximum radius R_m. Comparison of the exact numerical results with the approximate zeroth-order variational results and the analytical expressions obtained with several orders of perturbative expansion.

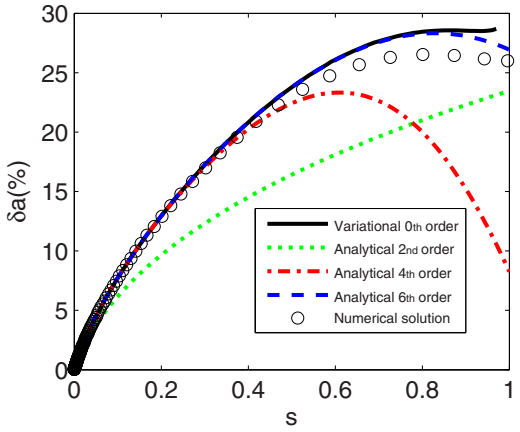

FIG. 7. (Color online) Excess of surface area δa along the constriction pathway. Comparison of the exact numerical results with the approximate zeroth-order variational results and the analytical expressions obtained with several orders of perturbative expansion.

Figure 6 shows the results for the analytic perturbative expressions corresponding to the volume increase. As with membrane dilation, the low-constriction regime described by the leading term is quite small ($s \leqslant 0.075$). The fourth-order perturbation [all terms in Eq. (22)] matches quite accurately the exact result (6% maximal error in describing the whole constriction pathway; see Fig. 6), even qualitatively describing the reduction of volume increase observed when approaching large constrictions ($s \to 1$). Higher order converges to the variational limit, but underestimates the volume increase even at relatively low constrictions ($s \geqslant 0.5$).

An interesting way of relating the increase in area and volume is to show the excess of surface area (see Fig. 7). The excess of surface area δa can be defined as the relative amount of surface area in excess of the minimal area required to enclose the volume of the vesicle, which is the surface area of the sphere with the same volume $A_{\text{sph}(V)}$. Thus,

$$\delta a = \frac{A(s) - A_{\text{sph}(V(s))}}{A_{\text{sph}(V(s))}}, \tag{23}$$

with $A_{\text{sph}(V)} = 6^{2/3}\pi^{1/3}V^{2/3}$. The accuracy of the results with the different approximations is the same as for the area and volume, the magnitudes from which it is derived. An interesting observation is that for high constriction, the amount of excess area approaches the value expected for a vesicle with the area and volume of two spheres of radius R_0, i.e., $A_{2\text{sph}} = 2(4\pi R_0^2)$ and $V_{2\text{sph}} = 2(4\pi R_0^3/3)$, which implies

$$\delta a = \frac{2\left(4\pi R_0^2\right)}{6^{2/3}\pi^{1/3}\left\{2\left[(4\pi/3)R_0^3\right]\right\}^{2/3}} - 1 = 2^{1/3} - 1 = 0.26 = 26\%,$$

in agreement with the limit of the exact numerical result in Fig. 7.

In terms of geometry, the previous results hold for shapes with the constraint to maintain the maximal radius R_m constant. However, other conditions such as constant area or constant volume could be additionally considered. In these cases, a redimensioning strategy can be addressed, as described

in previous work [9] defining a rescaling parameter λ as

$$\lambda_A(s) = \left[\frac{4\pi R_0^2}{A(s)}\right]^{1/2} \tag{24a}$$

if the area remains constant or as

$$\lambda_V(s) = \left[\frac{4\pi R_0^3/3}{V(s)}\right]^{1/3} \tag{24b}$$

if the volume remains constant. In these expressions, R_0 is the radius of the initial sphere with no constriction ($s = 0$). Now, in these cases, the parameter $R_m \neq R_0$ varies along the constriction pathway as

$$R_m(s) = \lambda_A(s) R_0 \tag{25a}$$

or as

$$R_m(s) = \lambda_V(s) R_0 \tag{25b}$$

in the constant area or constant volume constriction cases, respectively. For all the expressions, the subscript indicates what is kept constant. Note that at low constriction (limit $s \to 0$), $R_m = R_0$ for all of these cases. These rescaling parameters give the area during constant volume constriction as

$$A_V(s) = \lambda_V^2(s) A_{R_m}(s) \tag{26a}$$

and the volume during constant area constriction as

$$V_A(s) = \lambda_A^3(s) V_{R_m}(s), \tag{26b}$$

with area A_{R_m} and volume V_{R_m}. The results for constriction at constant maximum radius R_m are given by the expressions in Eqs. (20) and (22), respectively.

Figure 8 compares analytical, variational, and exact (numerical) results. It shows that only sixth-order analytical expressions give good estimations for all constrictions. It is important to clarify that these analytical expressions for λ_A and λ_V are obtained just using the corresponding analytical expressions for the area A and the volume V in Eqs. (24a) and (24b), respectively.

We recall from Ref. [9] that to change from one sphere to two spheres while keeping the same area requires a decrease in volume that gives $V/V_0 = 1/2^{1/2} \approx 0.71$; if the change is made while keeping the volume constant the increase in area gives $A/A_0 = 2^{1/3} \approx 1.26$. These arguments are in agreement with the values found in Fig. 8 for maximum constriction $s = 1$. However, these are extremal cases, and constant volume constriction is a closer idealization of the usual cytokinesis where intense membrane trafficking is known to play a relevant role [13,14], while constant area constriction could be an idealization of cases where membrane trafficking is inhibited, for example, through heat shocks [15,16]. The excess of surface area is dimensionless and therefore it is scale invariant, having the same values for all three cases of constriction (constant maximum radius, constant volume, and constant area), which we have considered.

4. *Stability coefficients*

Once geometry and energetics have been considered, we will address the question of the instability of the symmetrical constriction by calculating analytic expressions for the stability coefficients whose general definitions were previously given in Ref. [9]. The stability of a shape can be measured by introducing small changes on it and comparing its energy with the original one. When the constriction is equatorially symmetric, the constriction ring can be displaced a length Δx to give an asymmetrical shape (maintaining constant area or volume with respect to the symmetrical form). In terms of energy, this new shape can be expressed as

$$E_{\text{asym}}(s) \approx E_{\text{sym}}(s) + k_V \left(\frac{\Delta x}{R_0}\right)^2, \tag{27}$$

where R_0 is the radius of the corresponding sphere (at $s \to 0$, $R_0 = R_m$) and k_V the stability coefficient with units of energy (k_V for constant volume and k_A for constant area). Since E_m, L_m/R_m, V, and A are involved in their expressions, we will take advantage of the corresponding analytic formulas obtained here from the perturbative expansion to insert them in the general expressions for the coefficients. For instance, maintaining constant volume, the stability coefficient k_V in

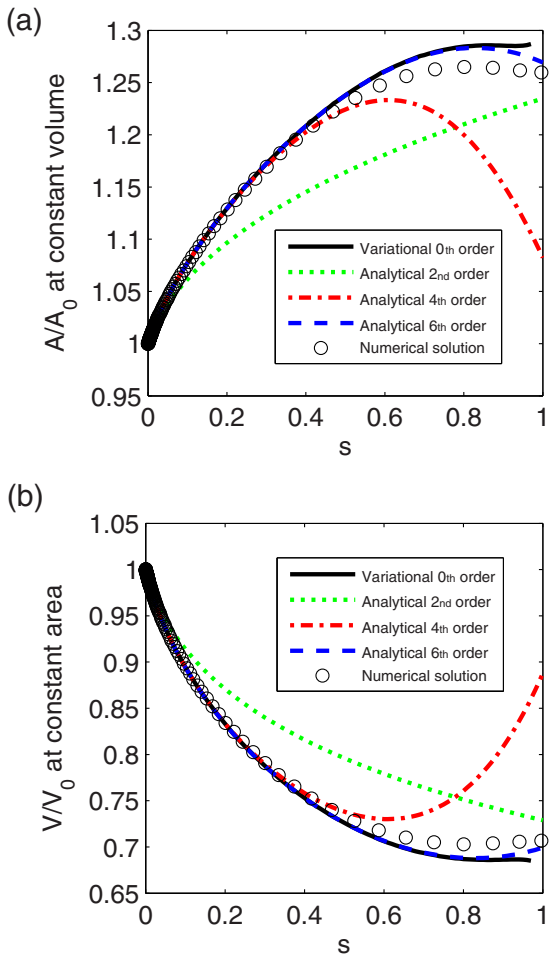

FIG. 8. (Color online) (a) Variation of area $A(s)/A_0$ along the constriction pathway maintaining constant volume. (b) Variation of volume $V(s)/V_0$ along the constriction pathway keeping the area constant. Comparison of the exact numerical results with the approximate zeroth-order variational results and the analytical expressions obtained with several orders of perturbative expansion.

Eq. (27) is given by [9]

$$k_V = -\frac{R_0^2}{2(1+\partial L_m/\partial R_m)^2}\left[\frac{\partial^2 E_m}{\partial R_m^2} - \frac{\partial E_m}{\partial R_m}\left(\frac{\partial^2 V}{\partial R_m^2}\Big/\frac{\partial V}{\partial R_m}\right)\right]. \tag{28}$$

In order to get the analytical formula for k_V one has to calculate the derivatives and insert them in Eq. (28) to give rise to the following expressions:

$$k_V \approx -\pi^2\kappa\left(\frac{R_0}{R_m}\right)^2\frac{k_V^N}{k_V^D}, \tag{29a}$$

$$k_V^N = \frac{6^{1/4}4}{3}\sqrt{s} + \frac{1+72\sqrt{6}}{48}\pi s + \frac{11\sqrt{6}+336}{48}6^{1/4}s^{3/2} - \frac{9113\sqrt{6}+69\,984}{41\,472}\pi s^2 + \cdots, \tag{29b}$$

$$k_V^D = \frac{6^{3/4}}{16}\pi^3\sqrt{s} + \sqrt{6}\pi^2 s + \frac{56\sqrt{6}\pi^2+2560-93\pi^2}{512} \times \pi 6^{1/4}s^{3/2} + \frac{16\pi^2\sqrt{6}-31\pi^2+128}{16}s^2 + \cdots. \tag{29c}$$

Although further simplification of these expressions is possible (using $s \ll 1$), we found that it reduced their range of validity.

The leading term defining the asymptotic regime converges to a constant limiting value at $s \to 0$ (where $R_0/R_m \approx 1$):

$$\lim_{s\to 0} k_V = -\frac{32}{3\pi}\sqrt{\frac{2}{3}}\kappa\left(\frac{R_0}{R_m}\right)^2 \approx -2.77\kappa. \tag{30}$$

Higher-order expressions are given in Appendix B. Figure 9 compares the results obtained with the different methods. The exact solution (calculated with the numerical method) gives negative values of the stability coefficient k_V, which indicates the unstable character of symmetric constriction at constant volume, a conclusion already raised in Ref. [9]. At small constriction, the exact numerical result points to a progressive destabilization of equatorial constriction in favor of axisymmetric configurations with a lower bending energy. The precision of the exact numerical solution is quite poor in this low-deformation regime, as evidenced by the high variability of the numerical values obtained. Variational methods also have precision problems for this magnitude. These precision problems seem to be related to the derivatives present in the expression defining k_V. However, the approximated analytic solutions offer a consistent description of this low-deformation regime, as a power-law approach $k_V \sim -s^{1/2}$, which converges down to the asymptotic limit $k_0 \approx k_V(s \to 0) \approx -2.77\kappa \approx -28k_BT$ (if $\kappa \approx 10k_BT$). For increasing constriction the instability is reduced and the stability coefficient approaches zero in the large-constriction limit ($k_V \to 0$ at $s \to 1$). In Fig. 9 we also see that the analytic expression progressively converges towards the zeroth-order variational solution. Close agreement is found between the exact results and the sixth-order perturbation along the whole range of constrictions.

Alternatively, if the constraint of constant area is considered, the corresponding stability coefficient k_A that would replace k_V in Eq. (27) takes the following form [9]:

$$k_A = -\frac{R_o^2}{2(1+\partial L_m/\partial R_m)^2}\left[\frac{\partial^2 E_m}{\partial R_m^2} - \frac{\partial E_m}{\partial R_m}\left(\frac{\partial^2 A}{\partial R_m^2}\Big/\frac{\partial A}{\partial R_m}\right)\right]. \tag{31}$$

Analogously, using the analytical expansions for E_m, L_m, and A, one gets the corresponding formula for k_A,

$$k_A \approx -\pi^2\kappa\left(\frac{R_0}{R_m}\right)^2\frac{k_A^N}{k_A^D}, \tag{32a}$$

$$k_A^N = \frac{6^{1/4}8}{3}\sqrt{s} + \frac{13+48\sqrt{6}}{24}\pi s + \frac{11\sqrt{6}+208}{24}6^{1/4}s^{3/2} - \frac{15\,245\sqrt{6}+38\,160}{20\,736}\pi s^2 + \cdots, \tag{32b}$$

$$k_A^D = \frac{6^{3/4}}{8}\pi^3\sqrt{s} + 2\sqrt{6}\pi^2 s + \frac{40\sqrt{6}\pi^2+2560-69\pi^2}{256} \times \pi 6^{1/4}s^{3/2} + \frac{128-25\pi^2+12\sqrt{6\pi^2}}{8}s^2 + \cdots, \tag{32c}$$

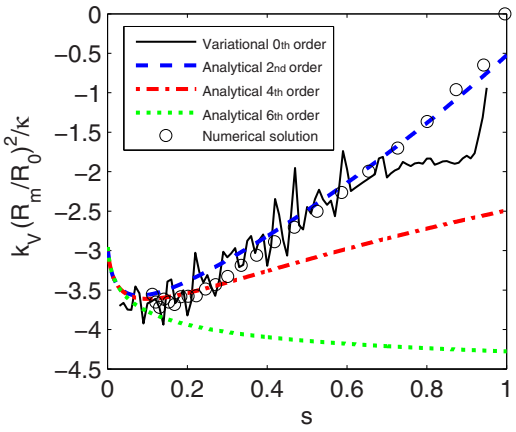

FIG. 9. (Color online) Stability coefficient k_V at all stages of constriction. Comparison of the exact numerical results with the approximate zeroth-order variational results and the analytical expressions obtained with several orders of perturbative expansion.

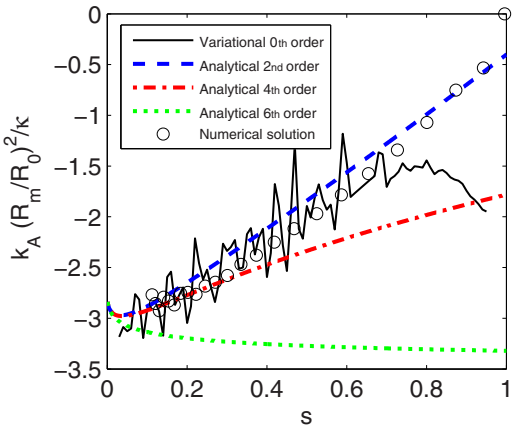

FIG. 10. (Color online) Stability coefficient k_A at all stages of constriction. Comparison of the exact numerical results with the approximate zeroth-order variational results and the analytical expressions obtained with several orders of perturbative expansion.

where the numerator (32b) and the denominator (32c) correspond to the fourth-order perturbative expansion. The analytic formula with higher orders is given in Appendix B.

A similar behavior is obtained for the stability coefficient at constant area k_A (see Fig. 10). The analytical expressions progressively approach the zeroth-order variational result and the sixth-order expression gives good agreement with the exact numerical results. Symmetric constriction is found unstable at low s ($k_A \approx -2.77\kappa$ at $s \to 0$), but becomes progressively less unstable with increasing constriction ($k_A \to 0$ at $s \to 1$). The values of these stability coefficients quantify the energy potential that additional mechanisms have to provide in order to stabilize symmetrical constriction.

IV. CONCLUSION

A procedure to find approximate analytical expressions for magnitudes involved in the constriction of a vesicle (or a simplified cell) has been developed. This procedure can be extended to other processes where the minimization of the bending energy determines the vesicle shape and the values of the main magnitudes. The procedure combines the perturbative expansion of the bending energy integrand for small deformations around a known solution with an ansatz for the deformation given by a simple family of functions that depends on one or several parameters. After the values of the parameters of the family of functions are determined variationally, i.e., by minimization of the bending energy. If the family of functions is simple enough, this computation can be done, obtaining analytical expressions. In our case, the analytic expressions take the form of a powerlike leading term in the constriction ratio s (with well-defined power-law exponents and amplitudes), which is corrected by a polynomic expansion in s. The resulting expressions are expected to hold better for small constrictions; however, in our case they are found to be good approximations even for medium or large constrictions, as in the case we shown in this paper. We have found that the fourth-order analytical expression gives a good approximation over the whole range of constrictions for the length of the constriction region L_m, the bending energy E_m, the constriction force F_c, the area A, and the volume V. However, a sixth-order approximation is required to have a good approximation for the excess of surface area δa, the change of area at constant volume, the change of volume at constant area, and the stability coefficients of symmetrical constriction (for both constant area k_A and constant volume k_V constriction).

The results found here correspond to the tensionless case $\Sigma = 0$, with no pressure difference $\Delta p = 0$, and for zero spontaneous curvature $C_0 = 0$, a case where the curvature energy is size invariant. Further extensions to cases where one or several of these restrictions are eliminated are more involved and are beyond the scope of the present paper. The analytical expressions provided give an easy and compact way to predict the requirement for successful symmetrical constriction. In particular, they indicate that constriction forces on the order of the piconewton (for $\kappa \approx 10 k_B T$) if the vesicles (or cells) are of micron size, while a mechanism that generates a stabilization potential with a constant of $\sim 30 k_B T$ or greater is needed to stabilize symmetric constriction. The results derived from this method can be used to guide the design of synthetic divisomes and the understanding of cell constriction. Other biological processes involving membrane bending (such as exocytosis and endocytosis) can also benefit from the insight these results and this method can provide.

ACKNOWLEDGMENTS

We gratefully acknowledge Elena Beltrán de Heredia Rodriguez for checking the results and the equations in the paper. This work was supported by Ministerio de Ciencia e Innovación (Spain) through Grants No. FIS2010-17440 (F.J.C.), No. FIS2012-35723 (F.M.), and No. CSD2007-0010 (F.M.) (the last one as part of the Consolider Ingenio en Nanociencia Molecular Grant); Ministerio de Economía y Competitividad (Spain) Grant No. FIS2009-14650-C02-01 (F.M); and Comunidad Autónoma de Madrid (Spain) Grant No. S2009MAT-1507 (F.M.). V.G.A.-V. acknowledges support from Ministerio de Educación Cultura y Deporte (Spain) through the Becas de Colaboración program.

APPENDIX A: NUMERICAL ALGORITHM USED FOR COMPARISON

We have used for comparison and to verify the analytical results the numerical procedure described in Refs. [19,20] by applying it to axisymmetric shapes stressed upon equatorial constriction while the maximum radius remains constant. In this method the profile is parametrized by its arc length S. The tilt angle $\psi(S)$ and the distance to the symmetry axis $X(S)$ are sufficient to determine the shape. The energy functional can be restated in terms of these coordinates and its derivatives with respect to S as

$$E_m = 2\pi\kappa \int_0^{S_1} L(\psi, \dot{\psi}, X, \dot{X}, \gamma) dS, \tag{A1}$$

where the integrand $L(\psi, \dot{\psi}, X, \dot{X}, \gamma)$ is

$$L \equiv \frac{X}{2}\left(\dot{\psi} + \frac{\sin\psi}{X}\right)^2 + \gamma(\dot{X} - \cos\psi). \tag{A2}$$

The first term reflects the mean curvature bending energy contribution. The last term involves the Lagrangian multiplier γ, which is introduced to maintain the relation $\dot{X} = \cos\psi$ between $X(S)$ and $\psi(S)$.

The corresponding Euler-Lagrange equations for the minimization of E_m are

$$\dot{\psi} = U, \tag{A3a}$$

$$\dot{U} = -\frac{U}{X}\cos\psi + \frac{\cos\psi \sin\psi}{X^2} + \frac{\gamma}{X}\sin\psi, \tag{A3b}$$

$$\dot{\gamma} = \frac{U^2}{2} - \frac{\sin^2\psi}{2X^2}, \tag{A3c}$$

$$\dot{X} = \cos\psi. \tag{A3d}$$

By applying the appropriate boundary conditions, the system of ordinary differential equations can be solved and the equilibrium shapes can be obtained. Note that this method includes

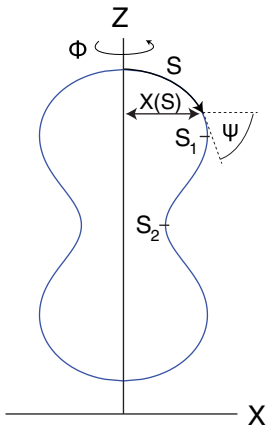

FIG. 11. (Color online) Scheme of the parametrization used for the numerical solution.

not only the constriction region, but also the description of the caps. In the case of constriction shapes, a set of conditions must be satisfied: At the beginning $X(0) = 0$, $\psi(0) = 0$, and $\gamma(0) = 0$; at the end of the cap $\psi(S_1) = \pi/2$, $X(S_1) = R_m$; at the constriction ring $\psi(S_2) = \pi/2$ and $X(S_2) = R_c$; and the corresponding symmetric boundary conditions are to the right of the constriction ring (see Fig. 11).

Maintaining the boundary conditions of radius R_m and R_c at S_1 and S_2 requires line tensions σ_m and σ_c, respectively. They act in opposite directions: Increasing σ_c forces R_c to decrease, thus increasing constriction, which requires an increase of σ_m to maintain constant R_m during the constriction process. The boundary matching conditions at these points S_1 and S_2 are given by [20]

$$\gamma^+ - \gamma^- = \Delta\gamma = \sigma, \tag{A4}$$

where the plus and minus superscripts refer to the value at the right and at the left of the boundary, respectively. The numerical solution is found by using the shooting method, adjusting the values of $U(0) = \dot{\psi}(0)$ and σ_m to make the solution verify the boundary conditions. In the case of symmetric constriction, the line tension at S_2 is given by $\sigma_c = 2\gamma(S_2)$.

APPENDIX B: ANALYTICAL EXPRESSIONS FOR TENSIONLESS VESICLES UP TO SIXTH-ORDER PERTURBATIVE EXPANSION

Including all the terms in the expressions below one gets the sixth-order expression in the perturbative expansion of the energy integrand, omitting the two last terms the fourth-order expressions, and omitting the four last terms the second order expressions:

$$L_m(s) = \frac{1}{2}6^{1/4}\pi R_m\sqrt{s}\left[1 - \frac{31\sqrt{6}+144}{576}s - \frac{1488\sqrt{6}+4327}{110\,592}s^2 - \frac{103\,939\sqrt{6}+291\,312}{21\,233\,664}s^3 - \frac{9\,364\,320\sqrt{6}+49\,536\,593}{24\,461\,180\,928}5s^4\right], \tag{B1}$$

$$\frac{E_m(s)}{8\pi\kappa} = 1 + \frac{1}{6}6^{1/4}\pi\sqrt{s} - \frac{11\sqrt{6}-48}{1152}6^{1/4}\pi s^{3/2} - \frac{1584\sqrt{6}-7439}{221\,184}6^{1/4}\pi s^{5/2} - \frac{2\,103\,403\sqrt{6}-11\,091\,600}{382\,205\,952}6^{1/4}\pi s^{7/2} - \frac{215\,694\,752\sqrt{6}-1\,247\,254\,465}{48\,922\,361\,856}6^{1/4}\pi s^{9/2}, \tag{B2}$$

$$F_c = \frac{\pi^2 6^{1/4}\kappa}{3R_m}\left[\frac{2}{\sqrt{s}} - \frac{11\sqrt{6}-48}{32}\sqrt{s} - \frac{1584\sqrt{6}-7439}{18\,432}5s^{3/2} - \frac{2\,103\,403\sqrt{6}-11\,091\,600}{31\,850\,496}7s^{5/2} - \frac{215\,694\,752\sqrt{6}-1\,247\,254\,465}{452\,984\,832}s^{7/2}\right], \tag{B3}$$

$$\frac{A(s)}{4\pi R_m^2} = 1 + \frac{\pi 6^{1/4}\sqrt{s}}{2} - \frac{7\sqrt{6}+432}{1152}\pi 6^{1/4}s^{3/2} + \frac{336\sqrt{6}+10\,121}{221\,184}\pi 6^{1/4}s^{5/2} + \frac{18\,341\sqrt{6}+154\,032}{42\,467\,328}\pi 6^{1/4}s^{7/2} - \frac{11\,201\,760\sqrt{6}+67\,237\,621}{48\,922\,361\,856}\pi 6^{1/4}s^{9/2}, \tag{B4}$$

$$\frac{V(s)}{\frac{4}{3}\pi R_m^3} = 1 + \frac{3}{4}\pi 6^{1/4}\sqrt{s} - \frac{31\sqrt{6}+720}{768}\pi 6^{1/4}s^{3/2} + \frac{4464\sqrt{6}+64\,793}{147\,456}\pi 6^{1/4}s^{5/2} - \frac{246\,787\sqrt{6}+1\,451\,184}{28\,311\,552}\pi 6^{1/4}s^{7/2} - \frac{50\,504\,544\sqrt{6}+270\,990\,229}{32\,614\,907\,904}\pi 6^{1/4}s^{9/2}, \tag{B5}$$

$$k_V \approx -\pi^2\kappa\left(\frac{R_0}{R_m}\right)^2\frac{k_V^N}{k_V^D}, \tag{B6a}$$

$$k_V^N = \frac{6^{1/4}4}{3}\sqrt{s} + \frac{1+72\sqrt{6}}{48}\pi s + \frac{11\sqrt{6}+336}{48}6^{1/4}s^{3/2} - \frac{9113\sqrt{6}+69\,984}{41472}\pi s^2 - \frac{31\,051+13\,200\sqrt{6}}{9216}6^{1/4}s^{5/2} - \frac{104\,556\sqrt{6}+723\,971}{663\,552}\pi s^3, \tag{B6b}$$

$$k_V^D = \frac{6^{3/4}}{16}\pi^3\sqrt{s} + \sqrt{6}\pi^2 s + \frac{56\sqrt{6}\pi^2+2560-93\pi^2}{512}\pi 6^{1/4}s^{3/2} + \frac{16\pi^2\sqrt{6}-31\pi^2+128}{16}s^2 + \frac{1\,327\,104-122\,016\pi^2+16\,399\sqrt{6}\pi^2-476\,160\sqrt{6}}{589\,824}\pi 6^{1/4}s^{5/2} + \frac{419\sqrt{6}-26\,748}{27\,648}\pi^2 s^3, \tag{B6c}$$

$$k_A \approx -\pi^2\kappa\left(\frac{R_0}{R_m}\right)^2\frac{k_A^N}{k_A^D}, \tag{B7a}$$

$$k_A^N = \frac{6^{1/4}8}{3}\sqrt{s} + \frac{13+48\sqrt{6}}{24}\pi s + \frac{11\sqrt{6}+208}{24}6^{1/4}s^{3/2} - \frac{15\,245\sqrt{6}+38\,160}{20\,736}\pi s^2 - \frac{24\,907+8976\sqrt{6}}{4608}6^{1/4}s^{5/2} - \frac{33\,032\sqrt{6}+348\,203}{331\,776}\pi s^3, \tag{B7b}$$

$$k_A^D = \frac{6^{3/4}}{8}\pi^3\sqrt{s} + 2\sqrt{6}\pi^2 s + \frac{40\sqrt{6}\pi^2+2560-69\pi^2}{256}\pi 6^{1/4}s^{3/2} + \frac{128-25\pi^2+12\sqrt{6}\pi^2}{8}s^2 + \frac{344\,064-26\,912\pi^2+5909\sqrt{6}\pi^2-134\,144\sqrt{6}}{98\,304}\pi 6^{1/4}s^{5/2} + \frac{4319\sqrt{6}-20\,592}{13\,824}\pi^2 s^3. \tag{B7c}$$

[1] T. D. Pollard and W. C. Earnshaw, *Cell Biology*, 2nd ed. (Saunders Elsevier, Philadelphia, 2008).

[2] J. Errington, R. Daniel, and D. Scheffers, Cytokinesis in bacteria microbiol, Microbiol. Mol. Biol. Rev. **67**, 52 (2003).

[3] C. Field, R. Li, and K. Oegema, Cytokinesis in eukaryotes: A mechanistic comparison, Curr. Opin. Cell Biol. **11**, 68 (1999).

[4] T. D. Pollard, Mechanics of cytokinesis in eukaryotes, Curr. Opin. Cell Biol. **22**, 50 (2010).

[5] D. Boal, *Mechanics of the Cell*, 2nd ed. (Cambridge University Press, Cambridge, 2012).

[6] R. A. Green, E. Paluch, and K. Oegema, Cytokinesis in animal cells, Annu. Rev. Cell Dev. Biol. **28**, 29 (2012).

[7] J. Sedzinski, M. Biro, A. Oswald, J.-Y. Tinevez, G. Salbreux, and E. Paluch, Polar actomyosin contractility destabilizes the position of the cytokinetic furrow, Nature (London) **476**, 462 (2011).

[8] T. D. Pollard and J.-Q. Wu, Understanding cytokinesis: Lessons from fission yeast, Nat. Rev. Mol. Cell Biol. **11**, 149 (2010).

[9] V. G. Almendro-Vedia, F. Monroy, and F. J. Cao, Mechanics of constriction during cell division: A variational approach, PLoS ONE **8**, e69750 (2013).

[10] G. Reshes, S. Vanounou, I. Fishov, and M. Feingold, Cell shape dynamics in escherichia coli, Biophys. J. **94**, 251 (2008).

[11] D. J. Morre, Membrane biogenesis, Annu. Rev. Plant Physiol. **26**, 441 (1975).

[12] A. Nohturfft and S. C. Zhang, Coordination of lipid metabolism in membrane biogenesis, Annu. Rev. Cell Dev. Biol. **25**, 539 (2009).

[13] R. Albertson, B. Riggs, and W. Sullivan, Membrane traffic: A driving force in cytokinesis, Trends Cell Biol. **15**, 92 (2005).

[14] E. Boucrot and T. Kirchhausen, Endosomal recycling controls plasma membrane area during mitosis, Proc. Natl. Acad. Sci. USA **104**, 7939 (2007).

[15] G. W. Niven, J. S. Morton, T. Fuks, and B. M. Mackey, Influence of environmental stress on distributions of times to first division in escherichia coli populations, as determined by digital-image analysis of individual cells, Appl. Environ. Microbiol. **74**, 3757 (2008).

[16] Z. Kutalik, M. Razaz, A. Elfwing, A. Ballagi, and J. Baranyi, Stochastic modelling of individual cell growth using flow chamber microscopy images, Int. J. Food Microbiol. **105**, 177 (2005).

[17] H.-J. Kim, H. J. Joo, Y. H. Kim, S. Ahn, J. Chang, K.-B. Hwang, D.-H. Lee, and K.-J. Lee, Systemic analysis of heat shock response induced by heat shock and a proteasome inhibitor MG132, PLoS ONE **6**, e20252 (2011).

[18] I. Hörger, F. Campelo, A. Hernández-Machado, and P. Tarazona, Constricting force of filamentary protein rings evaluated from experimental results, Phys. Rev. E **81**, 031922 (2010).

[19] U. Seifert, K. Berndl, and R. Lipowsky, Shape transformations of vesicles: Phase diagram for spontaneous-curvature and bilayer-coupling models, Phys. Rev. A **44**, 1182 (1991).

[20] F. Jülicher and R. Lipowsky, Shape transformations of vesicles with intramembrane domains, Phys. Rev. E **53**, 2670 (1996).

[21] M. Hu, J. J. Briguglio, and M. Deserno, Determining the gaussian curvature modulus of lipid membranes in simulations, Biophys. J. **102**, 1403 (2012).